ELSEVIER

Physica A 207 (1994) 28–36

PHYSICA A

Transport and diffusion in three-dimensional composite media

L.M. Schwartz[a], F. Auzerais[a], J. Dunsmuir[b], N. Martys[c], D.P. Bentz[c], S. Torquato[d]

[a]*Schlumberger-Doll Research, Old Quarry Road, Ridgefield, CT 06 877-4108, USA*
[b]*Exxon Research and Engineering Company, Route 22 East, Annandale, NJ 08 801, USA*
[c]*National Institute of Standards and Technology, Building Materials Division, Gaithersburg, MD 20899, USA*
[d]*Princeton Materials Institute, 70 Prospect Avenue, Princeton University, Princeton, NJ 08540-5211, USA*

Abstract

We will review recent progress in our understanding of classical transport in porous media. Theoretical concepts will be illustrated with two distinct kinds of calculations. The first involve the grain consolidation model and are based on a particular multisize packing of spherical grains. The computational methods developed here are sufficiently accurate that we propose to combine them with direct measurements of the pore and grain geometry based on X-ray microtomography. Our preliminary results indicate that this approach may well play an important part in future studies of transport in porous media.

1. Introduction

The transport properties of disordered porous media, such as reservoir rocks, catalytic beds, and ceramic composites are of importance in physics, chemical engineering, and materials science [1]. The essential feature of porous media is that they are composed of two interpenetrating, percolating phases, the pore and solid networks. In the last decade our understanding of electrical, fluid, and particle transport in such systems has grown enormously [1–13]. To a large extent, the essential parameters have been identified, exact and approximate relationships between them have been proposed, and the theory has been successfully compared with experiments and calculations on simple synthetic systems.

An important component of our work on transport theory has been the development of a family of three-dimensional model porous media. Broadly

SSDI 0378-4371(93)E0537-O

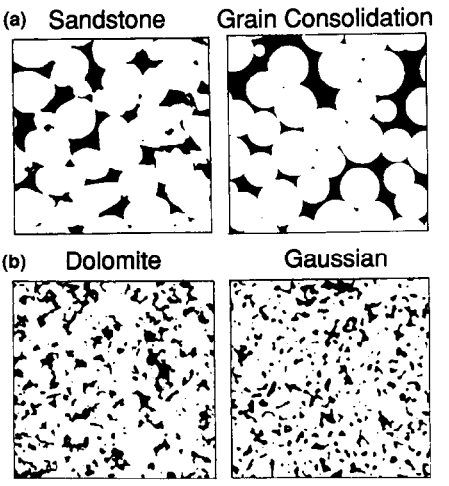

Fig. 1. (a) Left-hand panel shows a binary representation (black, pore; white, grain) of a thin-section optical photo of a quartzitic sandstone. Right-hand panel shows a section based on the consolidation of densely packed spherical grains; the model porosity has been adjusted to equal that of the sandstone. (b) Left-hand panel shows the corresponding binary representation of a thin-section optical photo of a crystalline dolomite. Right-hand panel shows a single plane from a Gaussian smoothed 3d model [7]; the model porosity has again been adjusted to equal that of the dolomite section.

speaking, these models fall into two categories: models based on grain packing [2,5] and models based on binary images [7] (Fig. 1). In section 2 the central equations describing transport in porous media will be reviewed and some results for a particular grain pack model will be summarized. In section 3 we present preliminary results related to what we believe will be an important part of the future of transport calculations in composite media viz. high-resolution microtomography [14]. In this technique three-dimensional X-ray attenuation maps are generated using synchrotron X-ray sources and digital panoramic electro-optical detectors. One can then replace synthetic images of the kind shown in Fig. 1b with experimental data and base transport calculations directly on the measured three-dimensional microgeometry.

2. Theoretical background

2.1. Electrical conductivity

Suppose we have a sample composed of an insulating porous material of length L, saturated with a single fluid whose conductivity takes the uniform value σ_{fl}. If an electrostatic potential difference, ΔU, is applied across the system, the local electrostatic potential, $U(\boldsymbol{r})$, satisfies Laplace's equation, $\nabla^2 U(\boldsymbol{r}) = 0$, with the boundary condition $\boldsymbol{E}(\boldsymbol{r}) \cdot \hat{\boldsymbol{n}} \equiv -\nabla U(\boldsymbol{r}) \cdot \hat{\boldsymbol{n}} = 0$ (at the pore grain interface), where $\hat{\boldsymbol{n}}$ is a unit normal vector directed into the grain space. The total current, $\boldsymbol{J}$, is then

obtained by integrating the local contributions, $\boldsymbol{j}(\boldsymbol{r}) \equiv \sigma_{\mathrm{fl}} \boldsymbol{E}(\boldsymbol{r})$, and the effective conductivity of the porous medium is $\sigma_{\mathrm{eff}} \equiv L|\boldsymbol{J}|/\Delta U$. Useful dimensionless parameters characterizing the effective resistance to current flow are the formation factor, F, and the tortuosity, α,

$$F \equiv \sigma_{\mathrm{fl}}/\sigma_{\mathrm{eff}} = \alpha/\phi = D_0/\phi D_\infty \,, \tag{1}$$

where the porosity, $\phi \equiv V_{\mathrm{pore}}/V_{\mathrm{total}}$, is the volume fraction associated with the pore space. In the last equality, the Einstein relation has been used to write F in terms of restricted diffusion [5,6].

Consider an ensemble of particles released in a three-dimensional pore space at $t = 0$. We can define a time-dependent diffusion constant, $D(t)$, by keeping track of the mean squared displacements,

$$D(t) = \langle |\boldsymbol{r}(t) - \boldsymbol{r}(0)|^2 \rangle / 6t \,. \tag{2}$$

As the particles diffuse through the pore space, the value of $D(t)$ will decrease from its initial value, D_0 (characteristic of the bulk pore fluid), to a final value, D_∞, determined by the network tortuosity. We emphasize that F, α and D_∞ are *scale-invariant* quantities; if we uniformly magnify or shrink the sizes of the pores and grains, leaving the porosity unchanged, their values are unaffected.

Nevertheless, the electrical conduction problem does provide a framework for the introduction of useful pore-size parameters. In the study of interfacial conduction a quantity that arises naturally is the Λ parameter [3],

$$\frac{\Lambda}{2} \equiv \frac{\int |\boldsymbol{E}(\boldsymbol{r})|^2 \, \mathrm{d}V_{\mathrm{p}}}{\int |\boldsymbol{E}(\boldsymbol{r})|^2 \, \mathrm{d}S} \neq \frac{V_{\mathrm{p}}}{S} \,. \tag{3}$$

Here V_{p} is the pore volume and S is the surface area of the pore–grain interface. (Note that in the special case in which the pores are cylindrical tubes of radius R, the electric field is uniform, and $\Lambda = R = 2V_{\mathrm{p}}/S$.) Regarding the inequality in Eq. (3), we emphasize that V_{p}/S is a *geometrical* length that can, in principle, be measured by stereological techniques. By contrast, Λ is a *dynamical* length determined by the solutions of Laplace's equation and cannot be measured by geometrical analysis [3]. Note that Λ is a length that is directly related to transport; regions of the pore space in which the electric field vanishes do not contribute to Λ; this length is, in some sense, a measure of the *dynamically connected* part of the pore space.

2.2. Hydrodynamical calculations

Given a sample of porous material of length L across which there is an applied pressure difference ΔP, the flow of a viscous fluid is described by Darcy's law [10,11],

$$V = -(k/\eta)\,\Delta P/L\,, \tag{4}$$

where η is the fluid viscosity, k is the permeability, and V is the macroscopic volumetric flux per unit area. Equation (4) is analogous to Ohm's law for the flow of electrical current, and k is the counterpart of the effective conductivity. We emphasize, however, that k depends on both the tortuosity of the pore space and on the absolute dimensions of the pores. Indeed, k has the dimensions of area and may be thought of as representing the cross section of an effective channel for fluid flow through the pore space. The Darcy equation defines k but does not provide a framework for the calculation of fluid flow. In the limit of slow incompressible flow, the Navier–Stokes equations reduce to the linear Stokes equations,

$$\eta\nabla^2\boldsymbol{v}(\boldsymbol{r}) = \nabla p(\boldsymbol{r})\,, \qquad \nabla\cdot\boldsymbol{v}(\boldsymbol{r}) = 0\,, \tag{5}$$

where $\boldsymbol{v}$ and p are, respectively, the local velocity and pressure fields, and η is the fluid viscosity. The fluid velocity must vanish at the pore–grain interface and a prescribed pressure difference at the inlet and outlet faces is assumed. With recent progress in the application of finite difference techniques to the solution of Stokes equations, the calculation of k in disordered two- and three-dimensional systems is now feasible [10,11]. In our discussion of Eq. (3) we noted that Λ is a length that is directly related to size of the pore space flow paths. Having made this observation, Johnson et al. [3] proposed the following approximate relation between Λ and k:

$$k \approx \phi\Lambda^2/8\alpha\,, \tag{6}$$

which may be viewed as a *dynamic* version of the Kozeny–Carmen estimate [10]

$$k \approx \phi(V_p/S)^2/2\alpha\,. \tag{7}$$

2.3. Magnetic resonance and diffusion

The characteristic times involved in the decay of nuclear magnetism in porous media are related to the dimensions of the pore space because of enhanced relaxation at the pore–grain interface [4,8,9]. We picture a layer of thickness h at this interface, within which the effective proton decay rate is γ_S. Clearly, when h is small, the physical influence of this layer depends only on the product $\rho \equiv h(\gamma_S - \gamma_B)$, where γ_B is the bulk decay rate. [In most systems of interest the pores are sufficiently small (and γ_S is sufficiently large) that bulk relaxation may safely be neglected.] The decay process within a given porous medium is then a function of ρ (which we assume to be constant) and the self-diffusion coefficient D_0 of the bulk fluid.

In nuclear magnetic relaxation measurements on porous media, the magnetization of nuclear spins, $M(t)$, is initially uniform throughout the pore space and its subsequent decay is described by the normal mode expansion

$$M(t) = M_0 \sum_{n=1}^{\infty} I_n \exp(-t/\tau_n) , \qquad M_0 = M(t \to 0^+) . \tag{8}$$

In this representation, the lifetimes, τ_n, and the amplitudes, I_n associated with each mode are functions of ρ, D_0 and, of course, the pore geometry. A quantity that emerges naturally is the mean lifetime $\langle \tau(\rho, D_0) \rangle$ [8,9],

$$\langle \tau(\rho, D_0) \rangle = \sum_{n=1}^{\infty} I_n(\rho, D_0)\, \tau_n(\rho, D_0) . \tag{9}$$

A principal reason for our interest in the above equations is that the quantities $\tau_1(\rho \to \infty, D_0)$ and $\langle \tau(\rho \to \infty, D_0) \rangle$ are related to the permeability through the rigorous inequalities [8]

$$k \leq \phi D_0 \langle \tau(\rho \to \infty, D_0) \rangle , \qquad k \leq \phi D_0 \tau_1(\rho \to \infty, D_0)/\alpha . \tag{10}$$

In Fig. 2 we compare four permeability estimates for a three-dimensional sphere pack model [13]. The present model comprises spheres with three diameters, chosen such that their volumes are in the ratio 1:10:100; the relative concentrations of each component are such as to guarantee three equal contributions to the solid volume fraction. Over the porosity range studied, it is clear that the Λ parameter estimates gives the best representation of permeability. The diffusion-based bounds (10) significantly overestimate the permeability. The first of these bounds is based on an estimate of the mean pore size and is not sensitive to the throats that, in fact, control transport. The quantity τ_1 is the longest of the

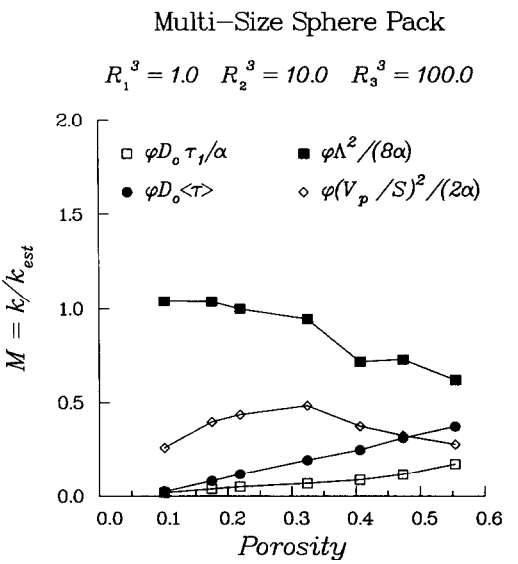

Fig. 2. Four permeability estimates are compared for a grain consolidation model based on a sphere pack with three grain sizes [13]. The porosity was varied by adding or subtracting δR to the radius of each sphere.

normal mode lifetimes and, as such, is determined by the largest pores in the system. Even though the second bound in Eq. (10) contains F, so that the influence of pore throats is represented, we see that it greatly overestimates the true permeability.

3. Microtomography and transport

Work of the kind described above is based on a (reasonable) guess as to the structure of porous media which is incorporated into a geometrical model of the kind shown in Fig. 1. Suppose, instead, that we could measure the microgeometry with sufficient resolution that our calculations could be based directly on the experimentally determined microstructure. In many cases this will be possible using advanced X-ray microtomography combined with high-intensity synchrotron X-ray sources [14].

To illustrate, we show in Fig. 3 part of a slice taken through a cylindrical plug (3 mm in diameter) of Fountainbleau sandstone. The voxel edge in this image is roughly 7.5 μm in length. The left-hand panel shows the gray-scale image that is typical of any single plane in the fully reconstructed three-dimensional data set. The first point to be made regarding the quality of these images is that experimental (i.e., buoyancy derived) porosity can be obtained directly from the gray-scale data. In Fig. 4 we show a graph of the computed porosity (obtained by constructing a histogram in which we count all voxels whose value is less than a given threshold), as a function of the threshold value. Naively, one might expect that (in a perfectly constructed image) such a graph would show a flat plateau dividing the pore and grain voxels. In fact, because the pore–grain interface will often pass through individual voxels, all intermediate gray levels will be represented. Thus, while the present data does not yield a simple plateau, we see that there is a well defined inflection point in the computed porosity whose value

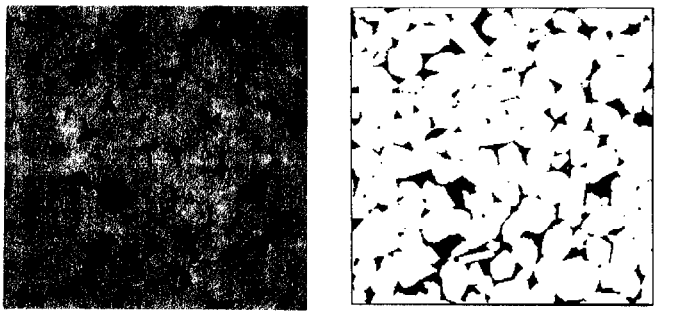

Fig. 3. Left-hand panel shows a gray-scale image obtained by X-ray microtomography with a voxel edge length of roughly 7.5 μm. The corresponding binary representation of this image is shown in the right-hand panel.

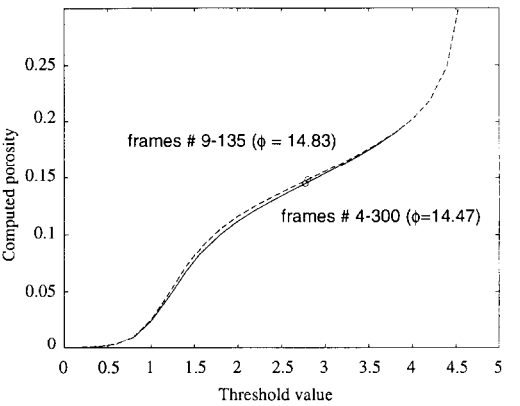

Fig. 4. Computed porosity is shown as a function of threshold value for the three-dimensional microtomography data on Fountainbleau sandstone. The solid curves sample the entire data set. The dashed curves show that essentially identical results are obtained from sampling less than half the image planes.

coincides with the experimentally determined porosity to within a fraction of a percent. Having so derived the porosity threshold, on the right-hand side of Fig. 3 we show a 288×288 binary representation of the original image. Note that the array of pore and grain shapes shown here is considerably more varied than in the upper panel of Fig. 1. We emphasize that the image shown in Fig. 3 must be viewed as part of a symmetric three-dimensional measurement in which the resolution between planes is equal to that within each plane.

At present, we have in place efficient codes to calculate the basic features of electrical conduction, fluid flow, and magnetic resonance in image-based models of porous media [5,11,12]. It is quite reasonable, therefore, to ask if these codes can be applied directly to the experimentally determined pore space microgeometry. We have completed only preliminary calculations to date. Working with a 200^3 subset of the measured data (i.e., with a cube that is roughly seven grains on a side) we have calculated the pore space correlation function, the electrical formation factor and the permeability. (The correlation function is of interest because its value at short distances is related to the V_p/S ratio which appears in Eq. (7) and which can be measured with comparable resolution by pulsed field gradient magnetic resonance [15,16].)

A comparison of our preliminary results with experiment is presented in Table 1. As we observed above, the agreement for the porosity is excellent. The permeability and V_p/S values are in reasonably good agreement with the measured values while the calculated formation factor is too high by roughly 65%. Generally, these results are quite encouraging. The fact that our calculations underestimate both the electrical conductivity and the permeability is to be expected because the image resolution does not allow for an accurate representation of the smaller pores and throats. On physical grounds we do not expect these

Table 1
Calculated values of ϕ, F, k and V_p/S based on microtomography data are compared with their experimentally determined counterparts. (The V_p/S value is derived from pulsed field gradient magnetic resonance measurements [16].)

	ϕ (%)	F	k (μm)^2	V_p/S (μm)
Measured	14.84	22.1	1.3	9.6
Calculated	14.47	37.8	1.0	12.2

channels to contribute greatly to fluid flow, but their effect on electrical transport can be quite substantial. We are in the process of refining our calculational techniques and are also working with data from other rock samples. We believe that the preliminary results presented here show that the combination of microtomographic data with transport calculations is feasible and that this synthesis offers exciting possibilities for future research.

Acknowledgements

Much of the research described in this paper has been carried out in collaboration with scientists who have either worked or are now working at Schlumberger-Doll Research. We have benefited greatly from these interactions and are pleased to acknowledge the contributions of J. Banavar, P. Crossley, D. Johnson, P. Sen and D. Wilkinson. We are also grateful to M. Hurlimann for allowing us to present one of his experimental results prior to publication.

References

[1] G.D. Cody, T.H. Geballe and P. Sheng, eds., Physical Phenomena in Granular Materials, Material Research Society Symposium Proceedings, vol. 195 (1990).
[2] J.N. Roberts and L.M. Schwartz, Phys. Rev. B 31 (1985) 5990;
L.M. Schwartz and S. Kimminau, Geophys. 52 (1987) 1402.
[3] D.L. Johnson, J. Koplik and L.M. Schwartz, Phys. Rev. Lett. 57 (1986) 2564;
L.M. Schwartz, P.N. Sen and D.L. Johnson, Phys. Rev. B 40 (1989) 2450.
[4] J.R. Banavar and L.M. Schwartz, Phys. Rev. Lett. 58 (1987) 1411;
C. Straley, A. Matteson, S. Feng, L.M. Schwartz, W.E. Kenyon and J.R. Banavar, Appl. Phys. Lett. 51 (1987) 1146.
[5] L.M. Schwartz and J.R. Banavar, Phys. Rev. B 39 (1989) 11965;
L.M. Schwartz, J.R. Banavar and B.I. Halperin, Phys. Rev. B 40 (1989) 9155.
[6] I.C. Kim and S. Torquato, J. Appl. Phys. 68 (1990) 3892.
[7] P.A. Crossley, L.M. Schwartz and J.R. Banavar, Appl. Phys. Lett. 59 (1991) 3553.
[8] S. Torquato, Phys. Rev. Lett. 64 (1990) 2644;
M. Avellaneda and S. Torquato, Phys. Fluids A 3 (1991) 2529.
[9] D. Wilkinson, D.L. Johnson and L.M. Schwartz, Phys. Rev. B 44 (1991) 4960.
[10] S. Kostek, L.M. Schwartz and D.L. Johnson, Phys. Rev. B 45 (1992) 186.

[11] N. Martys and E.J. Garboczi, Phys. Rev. B 46 (1992) 6080.
[12] L.M. Schwartz, D. Wilkinson, M. Bolsterli and P. Hammond, Phys. Rev. B 47 (1993) 4953.
[13] L.M. Schwartz, N. Martys, D.P. Bentz, E.J. Garboczi and S. Torquato, Phys. Rev. E 48 (1993) 4584.
[14] B.P. Flannery, H.W. Deckman, W.G. Roberge and K.L. D'Amico, Science 237 (1987) 1439.
[15] P.P. Mitra, P.N. Sen, L.M. Schwartz and P. Le Doussal, Phys. Rev. Lett. 68 (1992) 3555.
[16] M. Hurlimann, private communication.